24th COBEM - 2017

24th ABCM International Congress of Mechanical Engineering
December 3-8, 2017, Curitiba, PR, Brazil

COBEM-2017-2009
POROUS-MEDIA BRAKING OF ELECTROMAGNETIC STIRRING IN THE CONTINUOUS CASTING OF STEEL

M. Vynnycky[1,2]
[1]Division of Processes, Department of Materials Science and Engineering, KTH Royal Institute of Technology, Brinellvägen 23, 100 44 Stockholm, Sweden
[2]Department of Applied Mathematics and Statistics, Institute of Mathematical and Computer Sciences, University of São Paulo at São Carlos, PO Box 668, 13560-970 São Carlos, São Paulo, Brazil
michaelv@kth.se

Abstract. *Electromagnetic stirring (EMS) is applied at three locations in the continuous casting of steel, with a view to affecting the solidified crystal structure. At two of these, there is a significant mushy zone - a porous medium in which solid dendrites coexist with interdendritic melt. Whilst there exist numerous detailed magnetohydrodynamic models for the stirring of melt, both in this and other contexts, there has been no detailed treatment of the case where stirring occurs both in a melt and in an adjacent porous medium. This contribution provides a framework for such a model, starting with the case of rotary EMS applied to a round billet. In this case, the governing partial differential equations, which consist of Maxwell's equations and the turbulent Navier-Stokes equations with a Darcy-like damping term, reduce, under a number of assumptions, to just a fourth-order system of ordinary differential equations for the angular velocity and a function which describes the radial and angular magnetic field components, with the radial coordinate as the independent variable. Preliminary numerical results are given, as well as a comparison with the case when there is no mush.*

Keywords: *continuous casting, electromagnetic stirring, mushy zone*

1. INTRODUCTION

As noted in Tzavaras and Brody (1984), electromagnetic stirring (EMS) has been used in the continuous casting of steel slabs, blooms and billets since the mid-1970s as a way to control solidification structures, thereby increasing yield and productivity. In general, its purpose is to break up the columnar crystal structures that form during solidification, thereby promoting preferred equiaxed crystal structures.

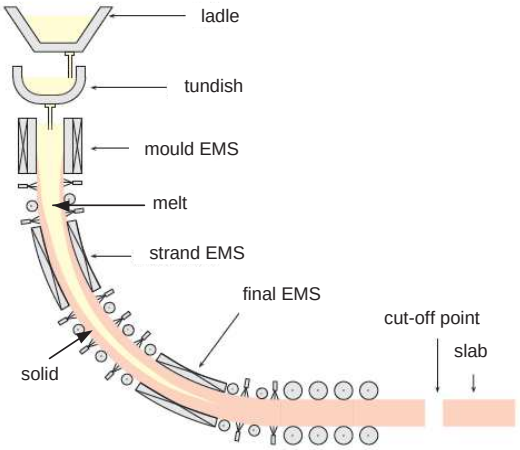

Figure 1. Schematic of the continuous casting process with EMS

As shown in Fig. 1, EMS is in general applied at three locations in the continuous casting process: in the mould region (M-EMS), further down along the strand (S-EMS) and in the final stirring region (F-EMS) where solidification is almost complete.

Moreover, there are in general three different modes in which electromagnetic stirring can be applied; these are shown

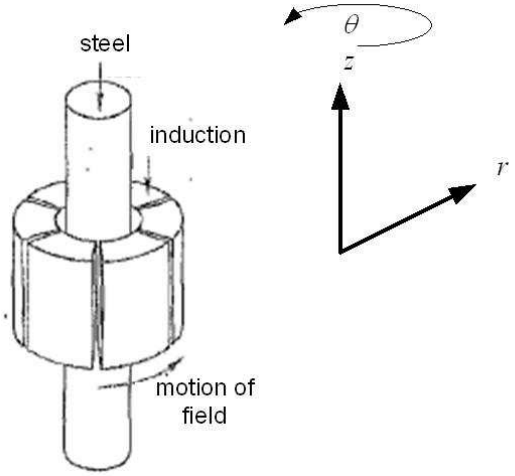

Figure 2. Schematic of an arrangement of an inductor around a circular steel strand for inducing rotating fields

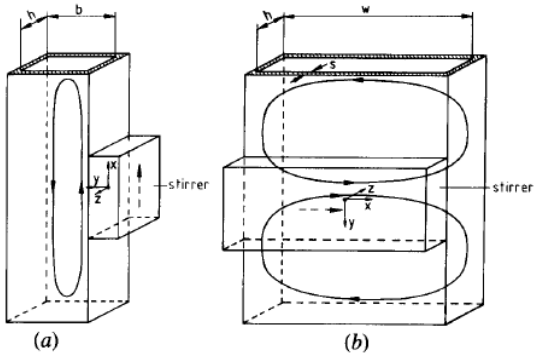

Figure 3. Longitudinal stirring of blooms and billets (a), and horizontal stirring of slabs (b)

in Figs. 2 and 3. Common to each case is that a magnetic field generated by coils that are situated around, or to the side of, the solidifying steel strand results in a Lorentz force which stirs the steel melt. However, there is no distinct front between the solid strand and the melt; between them, there is a porous medium, often referred to as a mushy zone, in which solid dendrites and interdendritic melt coexist. Consequently, EMS can affect the motion of this melt, but there may in turn be a braking effect as a result of the solid that is present.

In general, it is difficult to take measurements of what happens in this region; experimentally, the only possibility is to see the final solidified structure of the casting. For this reason, it is important to construct mathematical models that can attempt to describe what happens. In practice, this is a combination of momentum, heat and solute transfer occurring over solid, mush and liquid regions. In addition, it is necessary to take account of the thermodynamic equilibrium between solid and liquid phases in the mush, as well as attenuation of the magnetic field from the outer surface of the solidified steel towards the centre of the melt; these two effects required the use of the phase diagram for the steel alloy and the solution of Maxwell´s equations for the magnetic field quantities.

Although a fair amount of work was done early on in understanding the stirring of a melt (Tacke and Schwerdtfeger, 1979; Tacke *et al.*, 1981; Spitzer *et al.*, 1986; Dubke *et al.*, 1988a,b, 1991), the explicit effect of the mush was not taken into account. Moreover, although current-day software programs are able to take account of the mush, the effect of EMS on solute transport has yet to be explained fully. Thus, in this first step, we consider a model for stirring in the presence of a mushy zone, which will later serve to model the S-EMS and F-EMS regions.

2. MODEL EQUATIONS

We consider the simplest possible realistic case, which involves the use of a rotary stirrer on a round billet geometry; this is the configuration first shown in Fig. 2. In this particular case, it is possible to reduce to the problem so as to consider just a horizontal plane, as shown in Fig. 4, wherein molten melt occupies the region $0 < r < r_0$, mush occupies $r_0 < r < r_m$ and solid occupies $r_m < r < r_b$. Moreover, because the magnetic field in rotary EMS can be modelled as a wave in the

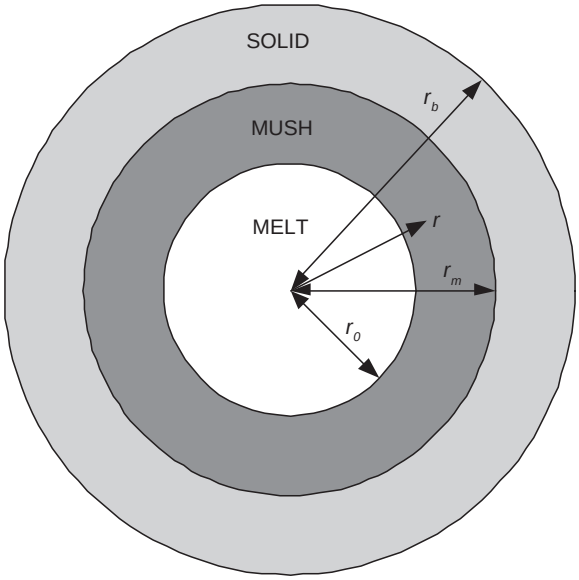

Figure 4. Schematic of circular solid, mush and melt regions

θ-direction at $r = r_b$ with a frequency that gives a time scale that is much shorter than that of relevance for casting, it possible to consider just the steady-state form of the mass and momentum equations, which take as input a time-averaged Lorentz force calculated from the transient Maxwell equations.

The continuity equation for the region in $0 < r < r_m$ is given in cylindrical (r, θ, z)-coordinates by

$$\frac{1}{r}\frac{\partial}{\partial r}\left(rv_r\right) + \frac{1}{r}\frac{\partial v_\theta}{\partial \theta} + \frac{\partial v_z}{\partial z} = 0, \tag{1}$$

where v_r, v_θ and v_z denote the r-, θ- and z-components of velocity. The conservation of momentum for $0 < r < r_m$ is given by

$$\rho\left\{v_r\frac{\partial v_r}{\partial r} + \frac{v_\theta}{r}\frac{\partial v_r}{\partial \theta} + v_z\frac{\partial v_r}{\partial z} - \frac{v_\theta^2}{r}\right\} = -\frac{\partial p}{\partial r} + \frac{1}{r}\frac{\partial}{\partial r}\left(r\tau_{rr}\right) + \frac{1}{r}\frac{\partial \tau_{\theta r}}{\partial \theta} - \frac{\tau_{\theta\theta}}{r} + \frac{\partial \tau_{zr}}{\partial z} + \bar{F}_r - \frac{\mu\chi v_r}{\kappa\left(\chi\right)}, \tag{2}$$

$$\rho\left\{v_r\frac{\partial v_\theta}{\partial r} + \frac{v_\theta}{r}\frac{\partial v_\theta}{\partial \theta} + v_z\frac{\partial v_\theta}{\partial z} + \frac{v_r v_\theta}{r}\right\} = -\frac{1}{r}\frac{\partial p}{\partial \theta} + \frac{1}{r^2}\frac{\partial}{\partial r}\left(r^2\tau_{r\theta}\right) + \frac{1}{r}\frac{\partial \tau_{\theta\theta}}{\partial \theta} + \frac{\partial \tau_{z\theta}}{\partial z} + \bar{F}_\theta - \frac{\mu\chi v_\theta}{\kappa\left(\chi\right)}, \tag{3}$$

$$\rho\left\{v_r\frac{\partial v_z}{\partial r} + \frac{v_\theta}{r}\frac{\partial v_z}{\partial \theta} + v_z\frac{\partial v_z}{\partial z}\right\} = -\frac{\partial p}{\partial z} + \frac{1}{r}\frac{\partial}{\partial r}\left(r\tau_{zr}\right) + \frac{1}{r}\frac{\partial \tau_{\theta z}}{\partial \theta} + \frac{\partial \tau_{zz}}{\partial z} + \bar{F}_z - \frac{\mu\chi v_z}{\kappa\left(\chi\right)}, \tag{4}$$

where ρ is the density of the melt, μ is its dynamic viscosity and $\kappa\left(\chi\right)$ is the permeability of the mushy region, which is taken to be a function of the liquid fraction, χ, and is given by the Kozeny-Carman relation,

$$\kappa\left(\chi\right) = \frac{\kappa_0\chi^3}{\left(1-\chi\right)^2}, \tag{5}$$

where κ_0 is a constant; although originally a relation used in the field of fluid dynamics to calculate the pressure drop of a fluid in laminar flow through a packed bed of solids (Carman, 1937), it has found extensive use in the modelling of flow through a solidifying mush (Ni and Beckermann, 1991; Reddy and Beckermann, 1997; Thevik *et al.*, 1999; Voller and Prakash, 1987; Du *et al.*, 2009; Haug *et al.*, 1995). Also, in equations (2)-(4), $\tau_{rr}, \tau_{\theta\theta}, \tau_{zz}, \tau_{rz}, \tau_{zr}, \tau_{\theta r}, \tau_{r\theta}, \tau_{\theta z}$ and $\tau_{z\theta}$ denote the components of the stress tensor, and are given by

$$\begin{aligned}
&\tau_{rr} = 2\frac{\partial v_r}{\partial r}, \quad \tau_{\theta\theta} = \frac{2\left(\mu+\mu_T\right)}{r}\left(\frac{\partial v_\theta}{\partial \theta} + v_r\right), \quad \tau_{zz} = 2\left(\mu+\mu_T\right)\frac{\partial v_z}{\partial z},\\
&\tau_{rz} = \tau_{zr} = \left(\mu+\mu_T\right)\left(\frac{\partial v_z}{\partial r} + \frac{\partial v_r}{\partial z}\right), \quad \tau_{\theta r} = \tau_{r\theta} = \left(\mu+\mu_T\right)\left(r\frac{\partial}{\partial r}\left(\frac{v_\theta}{r}\right) + \frac{1}{r}\frac{\partial v_r}{\partial \theta}\right),\\
&\tau_{\theta z} = \tau_{z\theta} = \left(\mu+\mu_T\right)\left(\frac{\partial v_\theta}{\partial z} + \frac{1}{r}\frac{\partial v_z}{\partial \theta}\right),
\end{aligned} \tag{6}$$

with μ_T as the turbulent viscosity. For this, we adopt the Prandtl mixing length hypothesis, setting

$$\mu_T = \sqrt{\rho \tau_{r\theta}} l_m, \tag{7}$$

where the quantity l_m is Nikuradse's mixing length (Tacke and Schwerdtfeger, 1979; Versteeg and Malalasekera, 2007),

$$l_m = r_* \left(0.14 - 0.08 \left(\frac{r}{r_*} \right)^2 - 0.06 \left(\frac{r}{r_*} \right)^4 \right). \tag{8}$$

Typically, for a pure melt, r_* would be interpreted as radius of the melt, so that $l_m = 0$ at $r = r_*$; here, since l_m must be used in (2)-(4), which must be solved in the liquid and mush regions, we will take $r_* = r_m$. Furthermore, in equations (2)-(4), $\bar{F}_r, \bar{F}_\theta$ and $\bar{F}_z$ denote the time-averaged components of the Lorentz force, which we write as F_r, F_θ and F_z and which are given by

$$F_r = J_\theta B_z - J_z B_\theta, \quad F_\theta = J_z B_r - J_r B_z, \quad F_z = J_r B_\theta - J_\theta B_r,$$

where (J_r, J_θ, J_z) is the electrical current density vector, $\mathbf{J}$, and (B_r, B_θ, B_z) is the magnetic flux density vector, $\mathbf{B}$; moreover, F_r, F_θ and F_z are related to $\bar{F}_r, \bar{F}_\theta$ and $\bar{F}_z$ by

$$\bar{F}_r = \frac{1}{2\pi/\omega} \int_0^{2\pi/\omega} F_r \mathrm{d}t', \quad \bar{F}_\theta = \frac{1}{2\pi/\omega} \int_0^{2\pi/\omega} F_\theta \mathrm{d}t', \quad \bar{F}_z = \frac{1}{2\pi/\omega} \int_0^{2\pi/\omega} F_z \mathrm{d}t',$$

where the integrals are taken with respect to time over one oscillation period, $2\pi/\omega$. At this point, it may appear that $\bar{F}_r, \bar{F}_\theta$ and $\bar{F}_z$ should all be functions of r, θ and z, but as a consequence of the boundary conditions to be specified later, they will only be functions of r.

To determine $\mathbf{J}$ and $\mathbf{B}$, we must solve Maxwell's equations in the magnetohydrodynamic (MHD) approximation, which consist of:

- the magnetic field constraint,

$$\nabla \cdot \mathbf{B} = 0; \tag{9}$$

- Ampere's law,

$$\mathbf{J} = \nabla \times \mathbf{H}, \tag{10}$$

  where $\mathbf{H}$ is the magnetic field strength, which is related to $\mathbf{B}$ by $\mathbf{B} = \eta \mathbf{H}$, where η is the magnetic permeability;

- Faraday's law,

$$\nabla \times \mathbf{E} = -\frac{\partial \mathbf{B}}{\partial t}, \tag{11}$$

  where t is time and $\mathbf{E}$ is the electric field;

- Ohm's law,

$$\mathbf{J} = \sigma \left(\mathbf{E} + \mathbf{v} \times \mathbf{B} \right), \tag{12}$$

  where σ is the metal electrical conductivity, which we take to be constant over the solid, mush and liquid phases, and $\mathbf{v} = \chi \left(v_r, v_\theta, v_z \right)$.

Manipulating (10)-(12), we arrive at

$$\sigma \eta \frac{\partial \mathbf{B}}{\partial t} = \nabla^2 \mathbf{B} + \sigma \eta \left\{ \left(\nabla \cdot \mathbf{B} + \mathbf{B} \cdot \nabla \right) \mathbf{v} - \left(\nabla \cdot \mathbf{v} + \mathbf{v} \cdot \nabla \right) \mathbf{B} \right\}, \tag{13}$$

whence, on using (1) and (9),

$$\sigma \eta \frac{\partial \mathbf{B}}{\partial t} = \nabla^2 \mathbf{B} + \sigma \eta \left\{ \left(\mathbf{B} \cdot \nabla \right) \mathbf{v} - \left(\mathbf{v} \cdot \nabla \right) \mathbf{B} \right\}; \tag{14}$$

note, however, that this must still be solved together with equation (9).

The above may be simplified in a self-consistent way by taking $v_r \equiv 0, v_z \equiv 0, v_\theta = v_\theta(r), p = p(r), B_z = 0$ and $\partial/\partial z = 0$ in equations (1)-(4), (9) and (14). We find that (1) and (4) are satisfied automatically, whereas (2) and (3) become

$$-\frac{\rho v_\theta^2}{r} = -\frac{\mathrm{d}p}{\mathrm{d}r} + \bar{F}_r, \tag{15}$$

$$0 = \frac{1}{r^2}\frac{\mathrm{d}}{\mathrm{d}r}\left(r^2(\mu+\mu_T)\left(\frac{\mathrm{d}v_\theta}{\mathrm{d}r} - \frac{v_\theta}{r}\right)\right) + \bar{F}_\theta - \frac{\mu\chi v_\theta}{\kappa(\chi)}, \tag{16}$$

respectively, with $\bar{F}_r$ and $\bar{F}_\theta$ being determined by using

$$F_r = -\frac{B_\theta}{r}\left(\frac{\partial}{\partial r}(rB_\theta) - \frac{\partial B_r}{\partial \theta}\right), \quad F_\theta = \frac{B_r}{r}\left(\frac{\partial}{\partial r}(rB_\theta) - \frac{\partial B_r}{\partial \theta}\right). \tag{17}$$

Equation (16), except for the last term on the right-hand side, is the same as that given in Tacke and Schwerdtfeger (1979), and can be solved first for v_θ, after which (15) can be solved for p. Also, B_r and B_θ satisfy

$$\frac{1}{r}\frac{\partial}{\partial r}(rB_r) + \frac{1}{r}\frac{\partial B_\theta}{\partial \theta} = 0, \tag{18}$$

$$\sigma\eta\frac{\partial B_r}{\partial t} = \frac{\partial^2 B_r}{\partial r^2} + \frac{1}{r}\frac{\partial B_r}{\partial r} + \frac{1}{r^2}\frac{\partial^2 B_r}{\partial \theta^2} - \frac{B_r}{r^2} - \frac{2}{r^2}\frac{\partial B_\theta}{\partial \theta} - \sigma\eta\frac{\chi v_\theta}{r}\frac{\partial B_r}{\partial \theta}, \tag{19}$$

$$\sigma\eta\frac{\partial B_\theta}{\partial t} = \frac{\partial^2 B_\theta}{\partial r^2} + \frac{1}{r}\frac{\partial B_\theta}{\partial r} + \frac{1}{r^2}\frac{\partial^2 B_\theta}{\partial \theta^2} - \frac{B_\theta}{r^2} + \frac{2}{r^2}\frac{\partial B_r}{\partial \theta} + \sigma\eta\left(B_r\frac{\partial}{\partial r}(\chi v_\theta) - \frac{\chi v_\theta}{r}\frac{\partial B_\theta}{\partial \theta}\right). \tag{20}$$

The boundary conditions for v_θ are then just

$$v_\theta = 0 \quad \text{at } r = r_0, \tag{21}$$

$$v_\theta = 0 \quad \text{at } r = 0. \tag{22}$$

Also, the only boundary condition prescribed on the magnetic field quantities is that for B_θ at the outer edge of the solid,

$$B_\theta = B_0\cos(\omega t - n\theta) \quad \text{at } r = r_b, \tag{23}$$

where n is the number of poles. In addition, we require

$$B_\theta \quad \text{finite} \quad \text{at } r = 0. \tag{24}$$

Although (23) is different to that in much earlier work (Tacke and Schwerdtfeger, 1979; Spitzer *et al.*, 1986), it was found in recent work to lead to a unique solution (Vynnycky, 2017); on the other hand, specifying B_r instead, as was done in (Tacke and Schwerdtfeger, 1979; Spitzer *et al.*, 1986), does not. Moreover, it makes no difference if one requires B_r or B_θ to be finite at $r = 0$; if one is finite, then so is the other.

3. NONDIMENSIONALISATION

Nondimensionalizing through

$$R = \frac{r}{r_b}, \quad V_\theta = \frac{v_\theta}{V}, \quad P = \frac{p}{\rho V^2}, \quad \bar{\mu}_T = \frac{\mu_T}{\mu}, \quad B_R = \frac{B_r}{B_0}, \quad B_\theta = \frac{B_\theta}{B_0},$$
$$\tau = \frac{\omega t}{2\pi}, \quad \bar{F}_R = \frac{\bar{F}_r}{B_0^2/r_b\eta}, \quad \bar{F}_\Theta = \frac{\bar{F}_\theta}{B_0^2/r_b\eta}, \quad \bar{\kappa} = \frac{\kappa}{\kappa_0}, \tag{25}$$

where V is a velocity scale that has to be determined, equations (15) and (16) become

$$-\frac{V_\theta^2}{R} = -\frac{\mathrm{d}P}{\mathrm{d}R} + \frac{Ha^2}{Re_m Re}\bar{F}_R, \tag{26}$$

$$0 = \frac{1}{R^2}\frac{\mathrm{d}}{\mathrm{d}R}\left((1+\bar{\mu}_T)R^2\left(\frac{\mathrm{d}V_\Theta}{\mathrm{d}R} - \frac{V_\theta}{R}\right)\right) + \frac{Ha^2}{Re_m}\bar{F}_\Theta - Da^{-1}\frac{\chi V_\theta}{\bar{\kappa}(\chi)}, \tag{27}$$

respectively, where Ha, Re, Re_m and Da denote the Hartmann, Reynolds, magnetic Reynolds and Darcy numbers, respectively, and are given by

$$Ha = B_0 r_b\sqrt{\sigma/\mu}, \quad Re = \rho V r_b/\mu, \quad Re_m = V r_b\eta\sigma, \quad Da = \kappa_0/r_b^2, \tag{28}$$

Parameter	**Value**
B_0	0.02 T
f	50 Hz
n	1
r_b	0.1 m
η	1.2566×10^{-6} V s $\mathrm{A}^{-1}\mathrm{m}^{-1}$
κ_0	10^{-8} m^2
μ	0.006 kg $\mathrm{m}^{-1}\mathrm{s}^{-1}$
ρ	7200 kg m^{-3}
σ	7.14×10^{5} A $\mathrm{V}^{-1}\mathrm{m}^{-1}$

Table 1. Model parameters

whereas equations (18)-(20) become

$$\frac{1}{R}\frac{\partial}{\partial R}\left(RB_R\right)+\frac{1}{R}\frac{\partial B_\theta}{\partial\theta}=0, \tag{29}$$

$$\Omega\frac{\partial B_R}{\partial\tau}=\frac{\partial^2 B_R}{\partial R^2}+\frac{1}{R}\frac{\partial B_R}{\partial R}+\frac{1}{R^2}\frac{\partial^2 B_R}{\partial\theta^2}-\frac{B_R}{R^2}-\frac{2}{R^2}\frac{\partial B_\theta}{\partial\theta}-Re_m\frac{\chi V_\theta}{R}\frac{\partial B_R}{\partial\theta}, \tag{30}$$

$$\Omega\frac{\partial B_\theta}{\partial\tau}=\frac{\partial^2 B_\theta}{\partial R^2}+\frac{1}{R}\frac{\partial B_\theta}{\partial R}+\frac{1}{R^2}\frac{\partial^2 B_\theta}{\partial\theta^2}-\frac{B_\theta}{R^2}+\frac{2}{R^2}\frac{\partial B_R}{\partial\theta}+Re_m\left(B_R\frac{\partial}{\partial R}\left(\chi V_\theta\right)-\frac{\chi V_\theta}{R}\frac{\partial B_\theta}{\partial\theta}\right), \tag{31}$$

where $\Omega=f\sigma\eta r_b^2$. Note that Vynnycky (2017) determined that $V\sim B_0 r_b/0.14\rho^{1/2}\eta^{1/2}r_*$.

Boundary conditions (21)-(24) are now

$$V_\theta=0 \quad \text{at } R=1, \tag{32}$$
$$V_\theta=0 \quad \text{at } R=0, \tag{33}$$

$$B_\theta=\cos\left(2\pi\tau-n\theta\right) \quad \text{at } R=R_b, \tag{34}$$

$$B_\theta \quad \text{finite} \quad \text{at } R=0. \tag{35}$$

By setting

$$B_R=-\frac{1}{R}\,\mathrm{Re}\left(n\mathrm{i}ae^{\mathrm{i}(2\pi\tau-n\theta)}\right), \quad B_\theta=-\,\mathrm{Re}\left(\frac{\mathrm{d}a}{\mathrm{d}R}e^{\mathrm{i}(2\pi\tau-n\theta)}\right),$$

equations (27) and (29)-(31) can be reduced to

$$0=\frac{1}{R^2}\frac{\mathrm{d}}{\mathrm{d}R}\left\{\left(1+\bar{\mu}_T\right)R^2\left(R\frac{\mathrm{d}V_\theta}{\mathrm{d}R}-\frac{V_\theta}{R}\right)\right\}+\left(\frac{Ha^2}{Re_m}\right)\frac{\Omega\pi}{R}\left(\mathrm{Re}\left(a\right)^2+\mathrm{Im}\left(a\right)^2\right)-Da^{-1}\frac{\left(1-\chi\right)^2V_\theta}{\chi^2}, \tag{36}$$

$$\frac{\mathrm{d}^2a}{\mathrm{d}R^2}+\frac{n^2}{R}\frac{\mathrm{d}a}{\mathrm{d}R}-\left(\frac{1}{R^2}+\mathrm{i}\left(2\pi\Omega-Re_m\frac{\chi V_\theta}{R}\right)\right)a=0; \tag{37}$$

note that (26) can be solved for P after V_θ and a have been determined. The boundary conditions for (36) and (37) are

$$V_\theta=0 \quad \text{at } R=1, \tag{38}$$
$$V_\theta=0 \quad \text{at } R=0, \tag{39}$$
$$\frac{\mathrm{d}a}{\mathrm{d}R}=-1 \quad \text{at } R=1, \tag{40}$$
$$a=0 \quad \text{at } R=0. \tag{41}$$

4. RESULTS

In order to fix ideas, we use input data from earlier work (Tacke and Schwerdtfeger, 1979); this is given in Table 1. In addition, here we simply prescribe values for r_0 and r_m, as well as the functional form for χ, in order to demonstrate how the Darcy-like term in (36) affects the profile for V_θ; note that, on using the parameters in Table 1, we have $Da \sim 10^{-6}$, so that this term will start to have an effect once χ is sufficiently smaller than one. We can also note that $Re_m \sim 0.1$ so that the velocity will not have much effect on the magnetic field. To proceed, we take simply a linear profile for χ in the form

$$\chi = \frac{r - r_m}{r_0 - r_m}.$$

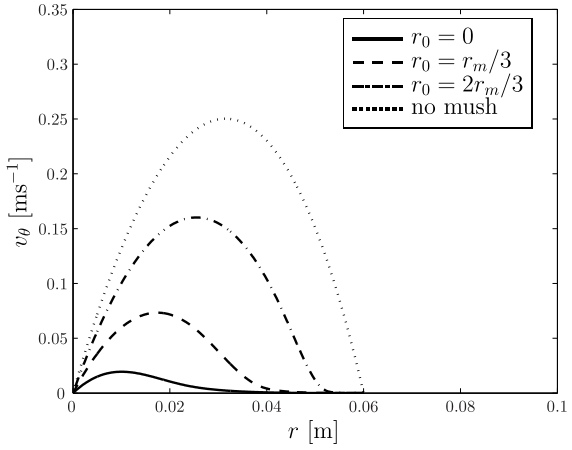

Figure 5. v_θ vs.r for $r_0 = 0, r_m/3, 2r_m/3$ and no mush, with $r_m = 0.06$ m

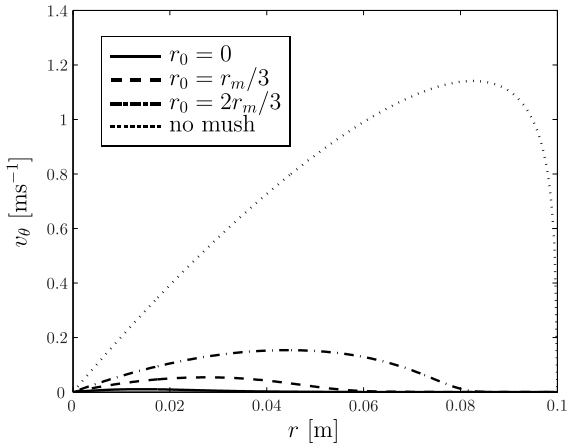

Figure 6. v_θ vs.r for $r_0 = 0, r_m/3, 2r_m/3$ and no mush, with $r_m = 0.1$ m

First, we take $r_m = 3r_b/5$; note that this value of r_m corresponds to the value used in Tacke and Schwerdtfeger (1979). Fig. 5 compares solution for V_θ when $r_0 = 0, r_m/3, 2r_m/3$ with the solution when the Darcy term is neglected completely, so that there is no mush. Here, the curve for no mush corresponds to that computed by Tacke and Schwerdtfeger (1979). It turns out that the profile given here has a maximum value that is around six times lower than that in Tacke and Schwerdtfeger (1979), which was around 1.5 ms^{-1}, as well as having its maximum displaced further away from $r = r_m$; it is not surprising that there is a difference, since the turbulence model used here is one of simplest as possible, whereas Tacke and Schwerdtfeger (1979) used a more sophisticated two-equation $k - W$ model. Nevertheless, even the value obtained here is not unreasonable in the context of electromagnetically-stirred melts. As regards the other curves in this plot, it is clear that the presence of the mushy layer reduces v_θ significantly: for example, for $r_0 = 0$, corresponding to mush occupying the entire region from $r = 0$ to r_m, the maximum value of v_θ is around 0.02 ms^{-1}.

Next, we take $r_m = r_b$, and plot the corresponding profiles in Fig. 6. Here, we find that the profile for the no-mush curve resembles much more closely that computed in Tacke and Schwerdtfeger (1979); even the maximum value for v_θ

compares favourably. There is also a proportionately greater drop in v_θ when going from the no-mush case to when $r_0 = 2r_m/3$.

5. CONCLUSIONS

Model equations have been presented to take account of the effect of the mushy zone on the electromagnetic stirring in the continuous casting of a round billet, with some preliminary calculations being carried out using parameters of industrial relevance.

The presented work can now be extended in a number of ways. First of all, although the casting velocity was not included in this analysis, it turns out that it can be incorporated without affecting the foregoing analysis. After that, it would be of interest to include an equation for the conservation of heat, so that the temperature and hence the liquid fraction are computed as part of the model, rather than the liquid fraction simply being prescribed. A nondimensional analysis of the type considered here will enable us to see whether the effect of the magnetic field affects the heat transfer in the problem, either through Joule heating or convection. Once these models are in place, it should be possible to assess the role of stirring in macrosegregation and crystal structure formation: with respect to white-band formation in the case of the former (Bridge and Rogers, 1984; Tacke *et al.*, 1981; Kor, 1982), and columnar-to-equiaxed crystal transition in the case of the latter.

A parallel line of activity will be to adapt these ideas to linear travelling magnetic fields for rectangular slabs, billets and blooms.

6. ACKNOWLEDGEMENTS

The author acknowledges the award of a visiting researcher grant from the University of São Paulo.

7. REFERENCES

Bridge, M.R. and Rogers, G.D., 1984. "Structural effects and band segregate formation during the electromagnetic stirring of strand-cast steel". *Met. Trans. B*, Vol. 15, pp. 581–589.

Carman, P.C., 1937. "Fluid flow through granular beds". *Trans. Inst. Chem. Engrs.*, Vol. 15, pp. 150–166.

Du, Q., Eskin, D.G. and Katgerman, L., 2009. "Numerical issues in modelling macrosegregation during DC casting of a multi-component aluminium alloy". *Int. J. Num. Meth. Heat Fluid Flow*, Vol. 19, pp. 917–930.

Dubke, M., Spitzer, K.H. and Schwerdtfeger, K., 1991. "Spatial-distribution of magnetic-field of linear inductors used for electromagnetic stirring in continuous-casting of steel". *Ironmak. Steelmak.*, Vol. 18, pp. 347–353.

Dubke, M., Tacke, K.H., Spitzer, K.H. and Schwerdtfeger, K., 1988a. "Flow fields in electromagnetic stirring of rectangular strands with linear inductors: Part I. Theory and experiments with cold models". *Metall. Mater. Trans. B*, Vol. 19B, pp. 581–593.

Dubke, M., Tacke, K.H., Spitzer, K.H. and Schwerdtfeger, K., 1988b. "Flow fields in electromagnetic stirring of rectangular strands with linear inductors: Part II. Computation of flow fields in billets, blooms, and slabs of steel". *Metall. Mater. Trans. B*, Vol. 19B, pp. 595–602.

Haug, E., Mo, A. and Thevik, H.J., 1995. "Macrosegregation near a cast surface caused by exudation and solidification shrinkage". *Int. J. Heat Mass Transfer*, Vol. 38, pp. 1553–1563.

Kor, G.J.W., 1982. "Influence of circumferential electromagnetic stirring on macrosegregation in steel". *Ironmak. Steelmak.*, Vol. 9, pp. 244–251.

Ni, J. and Beckermann, C., 1991. "A volume-averaged two-phase model for transport phenomena during solidification". *Metall. Mater. Trans. B*, Vol. 22B, pp. 349–361.

Reddy, A.V. and Beckermann, C., 1997. "Modeling of macrosegregation due to thermosolutal convection and contraction-driven flow in direct chill continuous casting of an Al-Cu round ingot". *Metall. Mater. Trans. B*, Vol. 28B, pp. 479–489.

Spitzer, K.H., Dubke, M. and Schwerdtfeger, K., 1986. "Rotational electromagnetic stirring in continuous-casting of round strands". *Metall. Mater. Trans. B*, Vol. 17, pp. 119–131. ISSN 0360-2141. doi:10.1007/BF02670825.

Tacke, K.H., Grill, A., Miyazawa, K. and Schwerdtfeger, K., 1981. "Macrosegregation in strand cast steel - computation of concentration profiles with a diffusion-model". *Arch. Eisenhüttenwes.*, Vol. 52, No. 1, pp. 15–20.

Tacke, K.H. and Schwerdtfeger, K., 1979. "Stirring velocities in continuously cast round billets as induced with rotating electromagnetic-fields". *Stahl und Eisen*, Vol. 99, pp. 7–12.

Thevik, H.J., Mo, A. and Rusten, T., 1999. "A mathematical model for surface segregation in aluminum direct chill casting". *Metall. Mater. Trans. B*, Vol. 39B, pp. 135–142.

Tzavaras, A.A. and Brody, H.D., 1984. "Electromagnetic stirring and continuous-casting - achievements, problems, and goals". *J. Metals*, Vol. 36, No. 3, pp. 31–37.

Versteeg, H. and Malalasekera, W., 2007. *An Introduction to Computational Fluid Dynamics: The Finite Volume Method*. Pearson, $2^{\rm nd}$ edition.

Voller, V.R. and Prakash, C., 1987. "A fixed grid numerical modelling methodology for convection-diffusion mushy region phase-change problems". *Int. J. Heat Mass Transfer*, Vol. 30, pp. 1709–1719.

Vynnycky, M., 2017. "On an anomaly in the modelling of electromagnetic stirring in continuous casting". Submitted to Metall. Mater. Trans. B.

8. RESPONSIBILITY NOTICE

The author is the only one responsible for the printed material included in this paper.